Science World Journal Vol. 20(No 2) 2025 https://dx.doi.org/10.4314/swj.v20i2.43
www.scienceworldjournal.org
ISSN: 1597-6343 (Online), ISSN: 2756-391X (Print)
Published by Faculty of Science, Kaduna State University

COMPUTING ENERGY FLUCTUATIONS IN DIATOMIC MOLECULES THROUGH THERMODYNAMIC PROPERTIES USING THE PARTITION FUNCTION APPROACH

*[1]P.J. Manga, [1]R.O. Amusat, [1]P.B. Teru, [1]Samaila H., [1]E.W. Likta, [1]Amina A. Dibal, [2]M.N. Yahaya, [3]Ngari A.Z., [4]Omolara Victoria Oyelade, [5]S.D. Buteh, [6]N.S. Gin, [7]Sheik Ubale Abdu, [8]Sabo Isyaku

[1]Department of Physics, University of Maiduguri, Borno State, Nigeria
[2]Department of Physics with Electronics, Federal University Birnin Kebbi, Kebbi State
[3]Department of Physics, Nigeria Army University, Biu, Borno State, Nigeria
[4]Department of Physics, Bingham University, Karu, Nasarawa State, Nigeria
[5]Department of Chemistry, Adamu Tafawa Balewa College of Education, Kangire, Bauchi
[6]Department of Chemistry, Federal University of Gashua, Yobe State, Nigeria
[7]Department of Fine and Applied Art, Aminu Saleh College of Education, Azare, Bauchi State
[8]Department of Physics, Federal University Dutse, Jigawa State, Nigeria

*Corresponding Author Email Address: 2016peterjohn@unimaid.edu.ng

ABSTRACT

This study presents a numerical and computational investigation into the energy fluctuations of three diatomic molecules—carbon monoxide (CO), hydrogen (H_2), and scandium hydride (ScH)—under a varying temperature parameter β based on two – dimension Schrödinger equation governed by Nikiforov – Uvarov Functional Analysis (NUFA) approach under the influence of magnetic field and magnetic flux. The numerical analysis indicates that when no external magnetic field is applied $B = 0T$ and $\emptyset_{AB} = 0$, the energy spectrum experiences a slight increase. However, a higher energy spectrum is observed when an external field is introduced at $\emptyset_{AB} = 9$ and $B = 9\,T.$ Examining the individual effects reveals that $\emptyset_{AB} = 9$ and $B = 0\,T$ have a somewhat stronger impact on the energy spectrum compared to $B = 0T,$ and $\emptyset_{AB} = 0$ has a limited effect on the overall energy spectrum. Additionally, it was numerically demonstrated that the energy levels remain consistent across three diatomic molecules, regardless of changes in the magnetic quantum number. Furthermore, shifts were noted in orbitals (s, p, d, f), which are uniformly affected by external variables. The values of these orbitals decrease as the orbital quantum number (n) increases, following the expected sequence: s > p > d > f. Computational findings, derived from a thermodynamic approach using partition analysis, show a reduction in the partition function when plotted against temperature, influenced by the magnetic field and flux. It was also observed that both molecules exhibit heightened energy fluctuations as the magnetic field strength and flux increase. The study underscores the critical role of external magnetic factors in shaping molecular energy behaviour through entropy, internal energy, free energy, specific heat capacity and energy fluctuation across various temperature ranges.

Keywords: Energy Fluctuation, Partition Function, Magnetic Quantum Number, Temperature Parameter and Nikiforov Uvarov Functional Analysis (NUFA) method.

INTRODUCTION

The quantum behaviour of diatomic molecules is dictated by the Schrödinger equation, which serves as a fundamental framework for understanding their energy states (Manga *et al*., 2023). Solving this equation for a specific molecular system yields energy eigenvalues. Crucial for determining thermodynamic properties such as internal energy, entropy, and heat capacity. These properties, in turn, impact energy fluctuations within the system (Manga *et al*., 2023).

A key tool for analysing these fluctuations is the partition function, a statistical mechanics approach that accounts for contributions from all possible energy states to the system's thermodynamic behaviour (Manga *et al*., 2023). By incorporating energy eigenvalues into the partition function, it becomes possible to quantify how thermodynamic properties drive energy variations in diatomic molecules (Manga *et al*., 2023).

Manga et al. (2021) employed a mathematical modelling approach using the partition function to examine energy fluctuations in diatomic molecules, with further analysis conducted on the exponential screened parametric plus Yukawa potential to determine molecular energy eigenvalues and thermodynamic properties. However, the findings were inconclusive due to limitations in representing energy fluctuations under an external magnetic field within the quantum mechanical framework (Manga *et al*., 2023). Therefore, it is essential to investigate bound state solutions for a two-dimensional nonrelativistic wave equation under this potential while considering the influence of both magnetic and Aharonov–Bohm ($\emptyset_{AB}$) fields (Ikot *et al*., 2021).

Recently, there has been increasing interest in solving the nonrelativistic Schrödinger wave equation in a two-dimensional setting under an external magnetic field to obtain exact bound state solutions for diatomic molecules (Abu-shady *et al*., 2023). This approach facilitates the determination of their thermodynamic properties and provides insights into their behaviour at different magnetic and principal quantum numbers within a given quantum mechanical system (Abu-shady *et al*., 2023).

Abu-shady *et al*., (2023) study on the hydrogen atom in a two-dimensional framework explored its behaviour under an external magnetic field. In his research, he calculated the energy eigenvalues of diatomic molecules by utilizing various reduced masses and nuclear atomic distances derived from spectroscopic data (Abu-shady *et al*., 2023). His findings led to the development of a straightforward ionization process, which is induced by microwave excitation to generate a circularly polarized wave. Abu-shady *et al*., (2023) study hydrogen atom in two-dimension suggested to external magnetic field in his finding he was able to compute energy eigenvalues for diatomic molecules using different reduced masses and nuclear atomic distance obtained from spectroscopic analysis (Abu-shady *et al*., 2023). His finding leads to a simple ionisation produce that is excited by microwave to form a circular polarised wave. Eshghi investigated the two-dimensional Schrödinger equation under the influence of an external magnetic field and Aharonov–Bohm ($\emptyset_{AB}$) flux, incorporating a position-dependent mass within a superposed potential combining Morse and Coulomb potentials (Manga *et al*., 2023). Additionally, the author examined the thermodynamic properties associated with this potential. Furthermore, Eshghi solved the two-dimensional wave equation for a charged particle with a position-dependent mass under the combined effects of the Hulthén and Coulomb potentials, influenced by both an external magnetic field and the Aharonov–Bohm ($\emptyset_{AB}$) flux field, to determine bound state energy eigenvalues and wavefunctions (Onate *et al*., 2023).

Manga *et al*., (2023) solved the three-dimensional Schrödinger equation for various diatomic molecules, including HgH, ZnH, CdH, HBr, and HF, to determine bound state energy eigenvalues and unnormalized wavefunctions (Manga *et al*., 2023). This was achieved using a modified exponential parametric plus Yukawa potential for different principal and azimuthal quantum numbers. Additionally, Umirzakov, (2019) extended this work by introducing the Aharonov–Bohm (AB) flux and an external magnetic field into the system. They formulated a generalized version of the equation incorporating a radial scalar power potential (RSPP) within a curvilinear coordinate framework. (Ikot *et al*., 2021), solved the two-dimensional Schrödinger wave equation (SWE) by considering various power penetration potentials under the influence of a magnetic field and magnetic flux. In the absence of a magnetic field, he computed the energy levels of certain diatomic molecules using different quantum mechanical models (Ikot *et al*., 2021). His study also examined the effect of the Aharonov–Bohm (AB) field, revealing a significant shift in energy levels. Additionally, he analysed its influence when $m \neq 0$ and compared it to the case when $m = 0$, concluding that the AB field provided a better fit than the magnetic field (Ikot *et al*., 2021).

This study aims to solve the two-dimensional Schrödinger wave equation using the Modified Tietz-Wei Potential (MTWP) model under the influence of an external magnetic field and magnetic flux. The solution approach is based on the Nikiforov–Uvarov functional analysis method. The derived equation will be utilized to determine energy eigenvalues and the partition function. These results will then be applied to compute various thermodynamic properties, including entropy, mean free energy, specific heat capacity and energy fluctuation.

Schrodinger equation with Modified Tiet-Wei Potential (MTWP) model explore to an external magnetic field

The Hamiltonian operator for a charged particle moving under the influence of a modified Tietz-Wei potential, while also being affected by AB flux (magnetic flux) fields, can be represented in cylindrical coordinates. Consequently, the Schrödinger wave equation, incorporating the effects of the modified Tietz-Wei potential, is formulated as in equation (1) (Umirzakov, 2019).

$$\left(i\hbar\vec{\nabla} + \frac{\ell}{\mathbb{C}}\vec{\mathcal{A}}\right)^2 \psi(\rho,\phi,\mathbb{z}) = 2\mu\left[\mathbb{E}_{nm} + D_0\left(\frac{1+e^{-2\vartheta r}}{1-e^{-2\vartheta r}}\right) + D_1\frac{e^{-2\vartheta r}}{r}\right]\psi(\rho,\phi,\mathbb{z}) \qquad (1)$$

The energy level, denoted as $\mathbb{E}_{nm}$ depends on the effective mass μ of the system. The vector potential, represented by $\overrightarrow{"\mathcal{A}"}$, is expressed as the sum of two components: $\vec{\mathcal{A}} = \vec{\mathcal{A}}_1 + \vec{\mathcal{A}}_2$. These components contain the azimuthal terms, as described in Ikot *et al*., (2021), and are influenced by an external magnetic field. The relations $\vec{\nabla} \times \vec{\mathcal{A}}_1 = \vec{\mathfrak{B}}, \vec{\nabla} \times \vec{\mathcal{A}}_2 = 0,$ hold, where $\vec{\mathfrak{B}}$ represents the magnetic field. The first component is given by $\vec{\mathcal{A}}_1 = \frac{\vec{\mathfrak{B}}\, e^{-2\vartheta r}}{1-e^{-2\vartheta r}}\widehat{\emptyset}$,while the second component, $\vec{\mathcal{A}}_2 = \frac{\emptyset_{AB}}{2\pi r}\,\widehat{\emptyset},$, accounts for the additional magnetic flux generated by a solenoid, with $\vec{\nabla}.\vec{\mathcal{A}}_2 = 0$. Consequently, the total vector potential takes the compact form given by equation (2) (Ikot et al., 2021).

$$\vec{\mathcal{A}} = \left(0, \frac{\vec{\mathfrak{B}}\, e^{-2\vartheta r}}{1-e^{-2\vartheta r}} + \frac{\emptyset_{AB}}{2\pi r}\,\widehat{\emptyset}, 0\right) \qquad (2)$$

$$\frac{1}{r^2} = \frac{4\vartheta^2 e^{-2\vartheta r}}{\left(1-e^{-2\vartheta r}\right)^2} \ggg \frac{1}{r} = \frac{2\,\vartheta\, e^{-2\vartheta r}}{1-e^{-2\vartheta r}} \qquad (3)$$

Consider a wave function expressed in cylindrical coordinates as $\psi(\rho,\phi) = \frac{1}{\sqrt{2\pi\ell}}e^{im\emptyset}R_{nm}(\ell)$, where mmm represents the magnetic quantum number. Substituting this wave function and the vector potential into equation (2), and applying the approximation introduced by Greene and Aldrich, as outlined in equation (3), we perform some straightforward algebraic manipulations. This leads us to derive the following second-order differential equation for the radial component (Ikot *et al*., 2021).

$$R''_{nm}(\vartheta) + \left[\frac{2\mu\mathbb{E}_{nm}}{\hbar^2} + \frac{2\mu}{\hbar^2}\left(D_0\left(\frac{1+e^{-2\vartheta r}}{1-e^{-2\vartheta r}}\right) + D_1\frac{e^{-2\vartheta r}}{r}\right) + \frac{m^2-1/4\,(4\vartheta^2)}{\left(1-e^{-2\vartheta r}\right)^2} - \varkappa\frac{(4\vartheta^2 w^2)}{\left(1-e^{-2\vartheta r}\right)^2}\left(\vec{\mathfrak{B}} + \frac{\emptyset_{AB}}{2\pi}\right) - \frac{\ell^2}{\hbar^2 c^2}\left(\frac{4\vartheta^2 w^2}{\left(1-e^{-2\vartheta r}\right)^2}\left(\vec{\mathfrak{B}} + \frac{\emptyset_{AB}}{2\pi}\right)^2\right)\right]R_{nm}(\vartheta) \qquad (4)$$

Where $\varkappa = \frac{\ell\, m}{\hbar\, c}$

For mathematical convenience, we introduce the following dimensionless variables

$$w^2\frac{\partial^2 R}{\partial w^2} + w\frac{\partial R}{\partial w} + \left(-\mathcal{E}_{nm} + B\left(D_0\left(\frac{1+w}{1-w}\right) + D_1\frac{2\,\vartheta\, w}{(1-w)}\right) - \frac{w^2 C}{(1-w)^2} - \frac{D\, w^2}{(1-w)^2} - \frac{E\, w^2}{(1-w)^2} - \frac{F\, w^2}{(1-w)^2} - \frac{G\, w^2}{(1-w)^2} - \frac{H\, w^2}{(1-w)^2}\right)R_{nm}(w) = 0 \qquad (5)$$

$$-\mathcal{E}_{nm} = \frac{\mu\mathbb{E}_{nm}}{2\vartheta^2\hbar^2}, B = \frac{\mu}{2\vartheta^2\hbar^2}, c = m^2 - 1/4, D = \varkappa = \frac{\ell\, m}{\hbar\, c}, E = \left(\vec{\mathfrak{B}} + \frac{\emptyset_{AB}}{2\pi}\right), F = \frac{\ell^2\vec{\mathfrak{B}}}{c^2\hbar^2}, G = \frac{\vec{\mathfrak{B}}\emptyset_{AB}}{\pi}, H = \frac{{\emptyset_{AB}}^2}{4\pi^2} \qquad (6)$$

Equation (5) is transformed to obtained a solution of second order hypergeometric form (Ding *et al*., 2011).

$$\frac{\partial^2 R}{\partial w^2} + \frac{(1-w)}{w(1-w)}\frac{\partial R}{\partial w} + \frac{1}{w^2(1-w)^2}\{(-\mathcal{E}_{nm} + B + BD_1 2\vartheta + C +$$

$$D + E + F + G + H)\, w^2 + (2\mathcal{E}_{nm} + BD_1 2\vartheta)\, w - \mathcal{E}_{nm} + BD_0\}R_{nm}(w) = 0 \quad (7)$$

The generalised hypergeometric equation is of the form.

$$\Psi'' + \frac{\Upsilon_1 - \Upsilon_2 v}{v(1-\Upsilon_3 v)}\Psi' + \frac{1}{v^2(1-\Upsilon_3)^2}\{-\mathfrak{H}_1 v^2 + \mathfrak{H}_2 v - \mathfrak{H}_3\}\Psi(v) = 0 \quad (8)$$

By applying NUFA method, we obtained the following (Ding *et al*., 2011).

$$\mathfrak{H}_1 = \mathcal{E}_{nm} + B + BD_1 2\vartheta + C + D + E + F + G + H \quad (10)$$

$$\mathfrak{H}_2 = 2\mathcal{E}_{nm} + BD_1 2\vartheta \quad (11)$$

$$\mathfrak{H}_3 = \mathcal{E}_{nm} + BD_0 \quad (12)$$

Let $\Upsilon_1 = \Upsilon_2 = \Upsilon_3 = 1$

$$\eth = \frac{1}{2}\left((1-\Upsilon_1) \pm \sqrt{(1-\Upsilon_1)^2 + 4\mathfrak{H}_3}\right) \quad (13)$$

$$\eth = \sqrt{\mathfrak{H}_3} \quad (14)$$

$$\eth^2 = \mathcal{E}_{nm} + BD_0 \quad (15)$$

$$\bar{\omega} = \frac{1}{2\Upsilon_1}\left((\Upsilon_3 + \Upsilon_1\Upsilon_3 - \Upsilon_2) \pm \sqrt{(\Upsilon_3 + \Upsilon_1\Upsilon_3 - \Upsilon_2)^2 + 4\left(\frac{\mathfrak{H}_1}{\Upsilon_3} + \Upsilon_3\mathfrak{H}_3 - \mathfrak{H}_2\right)}\right) \quad (16)$$

$$\bar{\omega} = \frac{1}{2}\left(1 + \sqrt{4(B + C + D + E + F + G + H + BD_0}\right) \quad (17)$$

$$\eth^2 + 2\eth\left(\bar{\omega} + \frac{1}{2}\left(\frac{\Upsilon_2}{\Upsilon_3} - 1\right) + \frac{n}{\sqrt{\Upsilon_3}}\right) + \left(\bar{\omega} + \frac{1}{2}\left(\frac{\Upsilon_2}{\Upsilon_3} - 1\right) + \frac{n}{\sqrt{\Upsilon_3}}\right)^2 + \frac{1}{4}\left(\frac{\Upsilon_2}{\Upsilon_3} - 1\right)^2 - \frac{\Upsilon_1}{\Upsilon_3^2} = 0 \quad (18)$$

$$\eth^2 = \left(\frac{\wp - BD_0 - (\bar{\omega}+n)^2}{2(\bar{\omega}+n)}\right)^2 \quad (19)$$

The solution for energy spectrum is given as follows.

$$\mathcal{E}_{nm} = \frac{2\vartheta^2\hbar^2 D_0 B}{\mu} - \frac{2\vartheta^2\hbar^2}{\mu}\left(\frac{\wp - BD_0 - (\bar{\omega}+n)^2}{2(\bar{\omega}+n)}\right)^2 \quad (20)$$

RESULTS AND DISCUSSION

Tables 2 to 5 present the calculated energy eigenvalues using Equation (20) for three different cases: $\vartheta = 1.9426$ for Hydrogen, $\vartheta = 2.2940$ for Co, $\vartheta = 1.5068$ for ScH and $\vartheta = 1.46102$ for ScF, as listed in Table 1. In the absence of both fields, degeneracy is observed. However, when only a magnetic field is applied, the energy eigenvalues decrease, and degeneracy is lifted (Reiss, 1980).

Table 1: The Results of Spectroscopic Analysis (Jia *et al*., 2012).
.

Parameters	H_2	Co	ScH
$\mu(amu)$	0.50391	6.86067	10.68277
$D_e(cm^{-1})$	38266	90540	36778.9
$\alpha(\dot{A}^{-1})$	1.9426	2.2940	1.5068

Table 2: Energy values for the Modified Tietz-Wei potential model considering the effects of an external magnetic field $B(T)$ and flux (ϕ_{AB}) for different magnetic quantum numbers**.**

H_2 Diatomic Molecule						
m	n	$Orbit$	$B = 0, \phi_{AB} = 0$	$B = 9, \phi_{AB} = 0$	$B = 0, \phi_{AB} = 9$	$B = 9, \phi_{AB} = 9$
0	0	s	2.28680	2.30529	2.38939	2.31358
	1	p	2.21537	2.23740	2.21837	2.24781
	2	d	2.12682	2.14986	2.12990	2.16113
	3	f	2.02130	2.04487	2.02597	2.05578
1	0	s	2.2871	2.30545	2.28967	2.31369
	1	p	2.21571	2.23759	2.21869	2.24795
	2	d	2.12717	2.15007	2.13023	2.16129
	3	f	2.02343	2.04570	2.02628	2.05594
−1	0	s	2.28710	2.30545	2.28967	2.31369
	1	p	2.21571	2.23759	2.21869	2.24795
	2	d	2.12717	2.15007	2.13023	2.16129
	3	f	2.02343	2.04507	2.02628	2.05594

It can be seen in Table 2 that there is a slight increase in energy, as seen in the first and second energy columns when B = 9 and ϕ_{AB} = 0. Similarly, when ϕ_{AB}= 9 and B= 0, as reflected in the first and third energy columns, energy increases across all orbitals. Furthermore, the influence of flux appears to be more pronounced than that of the magnetic field (Edet *et al*., 2021). The fourth energy column, which represents the combined effect of both parameters, shows that energy levels are generally higher compared to other cases, highlighting their interaction. Additionally, the energy variation across quantum states (m, n) remains consistent, with higher orbitals (p, d, f) exhibiting a similar response to the effects of the magnetic field $B(T)$ and flux (ϕ_{AB}) (Edet *et al.*, 2021).

Table 3: Energy values for the Modified Tietz-Wei potential model considering the effects of an external magnetic field $B(T)$ and flux (ϕ_{AB}) for different magnetic quantum numbers.

Co Diatomic Molecule						
m	n	$Orbit$	$B = 0, \phi_{AB} = 0$	$B = 9, \phi_{AB} = 0$	$B = 0, \phi_{AB} = 9$	$B = 9, \phi_{AB} = 9$
0	0	s	3.91762	3.95155	3.92130	3.96512
	1	p	3.86467	3.89807	3.86829	3.91144
	2	d	3.81089	3.84377	3.81446	3.85693
	3	f	3.75629	3.78864	3.75980	3.80159
1	0	s	3.91803	3.95194	3.92171	3.96551
	1	p	3.86507	3.89846	3.86869	3.91182
	2	d	3.81129	3.84415	3.81485	3.85730
	3	f	3.75668	3.78901	3.76019	3.80196
-1	0	s	3.91803	3.95194	3.92171	3.96551
	1	p	3.86507	3.89846	3.86869	3.91182
	2	d	3.81129	3.84415	3.81485	3.85730
	3	f	3.75668	3.78901	3.76019	3.80196

Table 3 illustrates that in the first column, energy increases when an external field is introduced at $B = 0$ and $\phi_{AB} = 0$. A more significant rise is observed when both fields are applied simultaneously at $B = 9$ and $\phi_{AB} = 9$. In the third column, where $B = 0$ and $\phi_{AB} = 9$, the energy is slightly higher than in the second column ($B = 9$ and $\phi_{AB} = 0$), suggesting that flux has a greater impact on energy than the magnetic field. Additionally, for different magnetic quantum numbers (m = 0, 1, -1), the energy levels remain nearly the same, indicating that energy variations primarily depend on flux and the magnetic field rather than the quantum number m (Edet *et al*., 2021).

Regarding orbital dependence, higher orbitals (p, d, f) exhibit energy shifts similar to those of lower orbitals, implying that external parameters influence all states consistently. However, energy values decrease as the orbital quantum number (n) increases, following the order s > p > d > f, which aligns with expected quantum mechanical behaviour. Lastly, the highest energy values appear in the final column at $B = 9$ and $\phi_{AB} = 9$, confirming the interactive effect between the magnetic field $B(T)$ and flux (ϕ_{AB}) $(Ettah, 2021)$.

Table 4: Energy values for the Modified Tietz-Wei potential model considering the effects of an external magnetic field $B(T)$ and flux (ϕ_{AB}) for different magnetic quantum numbers.

ScH Diatomic Molecule						
m	n	$Orbit$	$\vec{\mathfrak{B}} = 0, \phi_{AB} = 0$	$\vec{\mathfrak{B}} = 9, \phi_{AB} = 0$	$\vec{\mathfrak{B}} = 0, \phi_{AB} = 9$	$\vec{\mathfrak{B}} = 9, \phi_{AB} = 9$
0	0	s	2.09068	2.09282	2.09091	2.09368
	1	p	2.07633	2.07849	2.07656	2.07936
	2	d	2.06157	2.06375	2.06180	2.06464
	3	f	2.04640	2.04861	2.04664	2.04950
1	0	s	2.09071	2.09284	2.09094	2.09370
	1	p	2.07635	2.07851	2.07659	2.07939
	2	d	2.06159	2.06378	2.06183	2.06466
	3	f	2.04643	2.04864	2.04667	2.04953
-1	0	s	2.09071	2.09284	2.09094	2.09370
	1	p	2.07635	2.07851	2.07659	2.07939
	2	d	2.06159	2.06378	2.06183	2.06466
	3	f	2.04643	2.04864	2.04667	2.04953

From Table 4, it is evident that the energy values experience a slight increase when the magnetic field $B(T)$ and flux (ϕ_{AB}) are applied. The combined influence of $B = 9T$ and $(\phi_{AB}) = 9$ leads to higher energy values as the quantum number set (m, n) increases, following a specific order. The variation in energy between different configurations is minimal but follows a systematic pattern, suggesting a perturbative effect of $B(T)$ and flux (ϕ_{AB}). Additionally, for the magnetic quantum numbers $m = 1\ and\ m = -1$, the energy values remain identical, demonstrating symmetric behavior in the presence of the external magnetic field $B(T)$ and flux (ϕ_{AB}) $(\mathrm{Edet}\ et\ al., 2021)$.

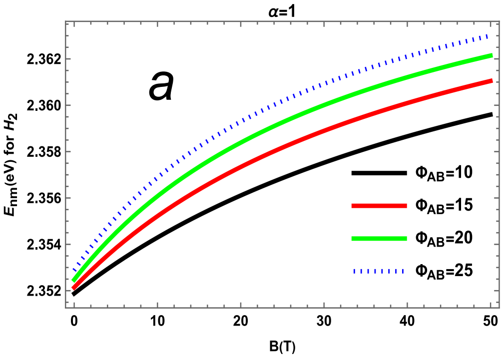

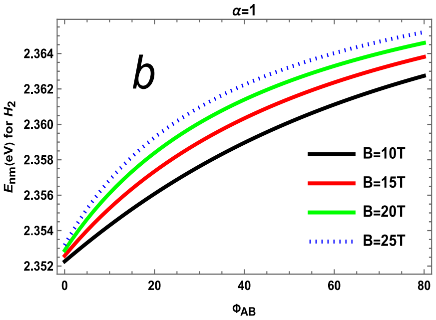

Figure 1: Computed energy eigenvalues for hydrogen diatomic molecules under varying B(T) and flux (ϕ_{AB}) (Edet $et\ al.$, 2021).

Figure 1 depict the energy eigenvalues of H_2 as a function of magnetic field B and flux (ϕ_{AB}). Plot 1(a) illustrates how energy values vary with the magnetic field B for different flux (ϕ_{AB}) values, ranging from 10 to 25. An increase in flux (ϕ_{AB}) corresponds to higher energy eigenvalues, with the highest flux value, represented by a dotted blue line, leading to the greatest energy levels (Edet *et al*., 2021). This indicates that both the magnetic field B and flux (ϕ_{AB}) contribute to energy shifts. Plot 1(b) demonstrates the dependence of energy eigenvalues on magnetic flux (ϕ_{AB}) for varying magnetic field strengths B between 10T and 25T. As the flux (ϕ_{AB}) increases, the energy eigenvalues also rise, indicating a direct relationship between flux (ϕ_{AB}) and energy eigenvalues. The system follows a consistent trend where stronger magnetic interactions result in increased energy, aligning with quantum mechanical predictions for magnetically influenced molecular systems (Edet *et al*., 2021).

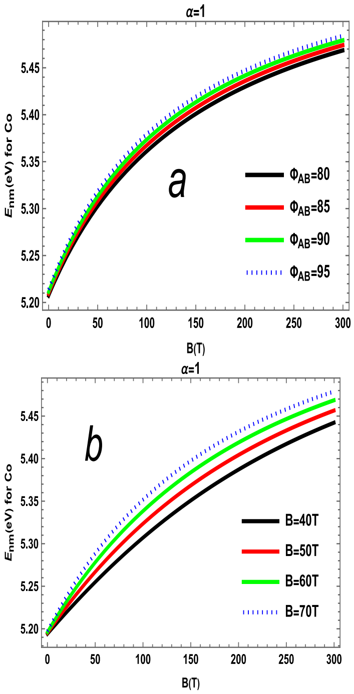

Figure 2: computed energy eigenvalues for carbon-mono-oxide diatomic molecules under varying B(T) and flux (ϕ_{AB}) (Edet $et\ al.$, 2021).

Figure 2 illustrates the algebraic influence of the magnetic field B and flux (ϕ_{AB}) on the energy eigenvalues of the Modified Tietz-Wei Potential (MTWP). In plot 1(a), the energy eigenvalues increase rapidly at low magnetic field B values and gradually stabilize as B increases. This trend is observed for different flux values (ϕ_{AB}=80, 85, 90 and 95) with higher flux (ϕ_{AB}) values corresponding to greater energy levels. Similarly, plot 2(b) demonstrates the relationship between energy eigenvalues and magnetic flux for various magnetic field strengths $(B = 40\ T, 50\ T, 60\ T\ \&\ 70\ T)$. As flux increases, the highest energy values are recorded at B=$60 - 70\ T$ reinforcing the notion that a stronger magnetic field enhances energy eigenvalues (Edet *et al*., 2021).

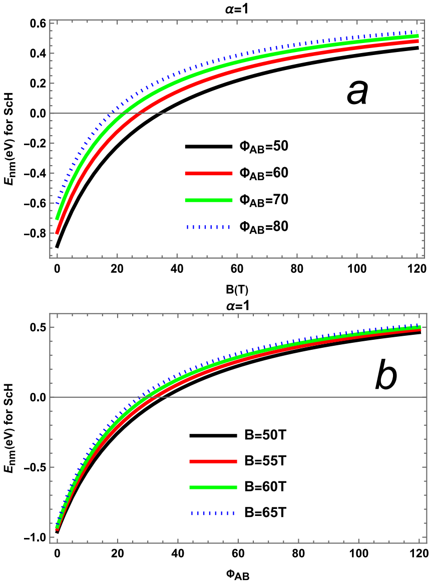

Figure 3: computed energy eigenvalues for Scandium Hydride diatomic molecules under varying $\vec{\mathfrak{B}}$ (T) and flux (ϕ_{AB}) (Onate $et\ al.$, 2021).

Figure 3 depicts the combined effect of the magnetic field and flux on Scandium Hydride. Plot 3(a) illustrates the variation of energy eigenvalues with the magnetic field for different flux values $(\phi_{AB} = 50, 60, 70\ and\ 80)$. At lower magnetic field strengths, the energy eigenvalues increase sharply before gradually stabilizing as B (T) continues to rise. Higher flux values correspond to greater energy levels, indicating that an increase in flux leads to higher energy eigenvalues (Onate *et al*., 2021).

Plot 3(b) demonstrates the relationship between energy eigenvalues and magnetic flux for different magnetic field strengths $(B = 50\ \mathrm{T}, 55\ \mathrm{T}, 60\ \mathrm{T}\ \mathrm{and}\ 65\ \mathrm{T})$. As flux increases, energy eigenvalues also rise, confirming a direct correlation between flux and energy. The highest magnetic field value B=65 T results in the maximum energy eigenvalues, reinforcing the idea that stronger magnetic fields enhance energy levels. This highlights the significant role of magnetic interactions in influencing the system's energy behaviour (Onate *et al*., 2021).

Thermodynamic Properties

In this section, the thermodynamic properties of the potential model were evaluated. These properties can be derived using the exact partition function as follows (Onate *et al*., 2021).

$$Z(\beta) = \sum_{n=0}^{\lambda} e^{-\beta E_n} \tag{21}$$

Where λ is an upper bound of the vibrational quantum number deduced from $\frac{dE_n}{d_n} = 0$, $\beta = \frac{1}{KT}$ where k and T are Boltzmann constant and temperature respectively. The summation can be replaced with an integral (Onate *et al*., 2021).

$$Z(\beta) = \int_0^{\lambda} e^{-\beta E_n}\, dn \tag{22}$$

The energy equation can be expressed in terms of a partition function as follows (Onate *et al*., 2021).

$$Z = e^{-\frac{\beta}{2}(K_3K_2+2K_1)} \int_0^{\lambda} e^{-\frac{\beta}{4}\left(\frac{K_3^2 K_2}{P^2} + K_2P^2\right)}\, dP \tag{23}$$

Z=

$$\frac{e^{-\frac{1}{2}\sqrt{-\beta K_2}\sqrt{-\beta K_2K_3^2}-\frac{1}{2}\beta K_2(2+K_3)}\sqrt{\pi}\left(1+e^{\sqrt{-\beta K_2}\sqrt{-\beta K_2K_3^2}}\left(-1+\mathrm{Erf}\left[\frac{P^2\sqrt{-\beta K_2}+\sqrt{-\beta K_2K_3^2}}{2P}\right]\right)+\mathrm{Erf}\left[\frac{1}{2}P\sqrt{-\beta K_2}-\frac{\sqrt{-\beta K_2K_3^2}}{2P}\right]\right)}{2\sqrt{-\beta K_2}} \tag{24}$$

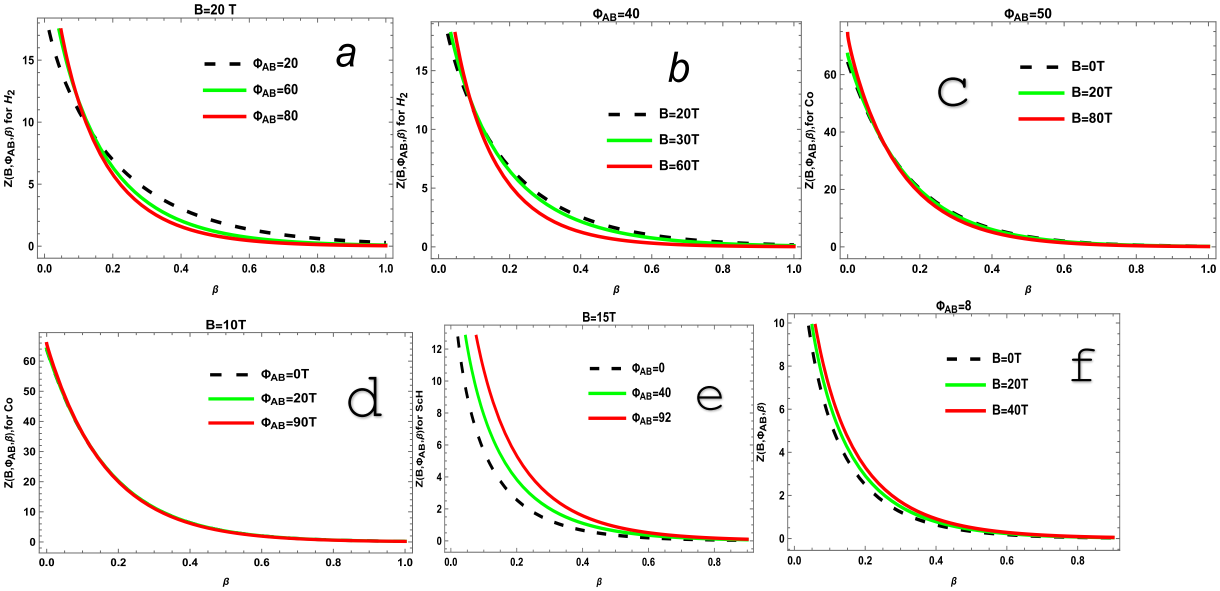

Figure 4: computed Partition Function for three diatomic molecules under varying $\overrightarrow{\mathfrak{B}}$ (T) and flux (ϕ_{AB}).

As shown in Plot 4a, when the magnetic field is held constant at (B=20 T), increasing the magnetic flux (ϕ_{AB}) results in a noticeable decrease in partition function values, particularly at low β (indicating high temperatures). In Plot 4b, with ϕ_{AB} fixed at 40, a gradual decline in the partition function is observed as the magnetic field increases from 20 T to 60 T. Similarly, plot 4c demonstrates that raising the magnetic field strength slightly lowers the partition function when the flux is kept constant at $\phi_{AB} = 50$.Plot 4d reveals that under a constant magnetic field of B=10 T, varying ϕ_{AB} produces almost overlapping curves, suggesting that changes in magnetic flux have minimal effect at lower magnetic field strengths. In Plot 4e, with B=15 T fixed, the curves show greater separation, indicating that magnetic flux has a more pronounced impact at this field strength. Finally, plot 4f, where $\phi_{AB} = 8,$ is held constant, shows that the partition function steadily decreases as the magnetic field increases, with clear distinctions between the curves (Onate *et al.*, 2021).

Vibrational Mean Internal Energy deduced from partition function

The internal energy of diatomic molecules, as obtained from the partition function, is essential for understanding their thermodynamic characteristics. It represents the cumulative energy from different molecular motions—especially vibrational, rotational, and translational—and shows how this energy is distributed across available energy levels (Onate *et al.*, 2021). By analyzing the partition function, one can examine how temperature and external influences, such as magnetic fields or flux, affect the energy states of the molecules and determine related properties like free energy, entropy and heat capacity (Onate *et al.*, 2021).

The mean vibrational internal energy is express as (Onate *et al.*, 2021)

$$U(\beta) = \frac{-\partial lnZ(\beta)}{\partial\beta} \Longrightarrow \frac{1}{4}\left(A + \frac{B+C}{\sqrt{\pi}\left(1-e^{\sqrt{-\beta K_2}\sqrt{-\beta K_2K_3^2}}+e^{\sqrt{-\beta K_2}\sqrt{-\beta K_2K_3^2}}\mathrm{Erf}\left[\frac{P^2\sqrt{-\beta K_2}+\sqrt{-\beta K_2K_3^2}}{2P}\right]+\mathrm{Erf}\left[\frac{1}{2}P\sqrt{-\beta K_2}-\frac{\sqrt{-\beta K_2K_3^2}}{2P}\right]\right)\sqrt{-\beta K_2}\sqrt{-\beta K_2K_3^2}}\right) \tag{25}$$

$$A= \frac{2}{\beta} - 4K_1 - 2K_2K_3 + \frac{2\sqrt{-\beta K_2}\sqrt{-\beta K_2K_3^2}}{\beta} \tag{26}$$

$$B = -4e^{\sqrt{-\beta K_2}\sqrt{-\beta K_2K_3^2}}\sqrt{\pi}\beta\left(-1 + \mathrm{Erf}\left[\frac{P^2\sqrt{-\beta K_2}+\sqrt{-\beta K_2K_3^2}}{2P}\right]\right)K_2^2K_3^2 \tag{27}$$

$$C=4e^{\frac{1}{4}\left(2\sqrt{-\beta K_2}\sqrt{-\beta K_2K_3^2}+\frac{\beta K_2(P^4+K_3^2)}{P^2}\right)}PK_2\sqrt{-\beta K_2K_3^2} \qquad (28)$$

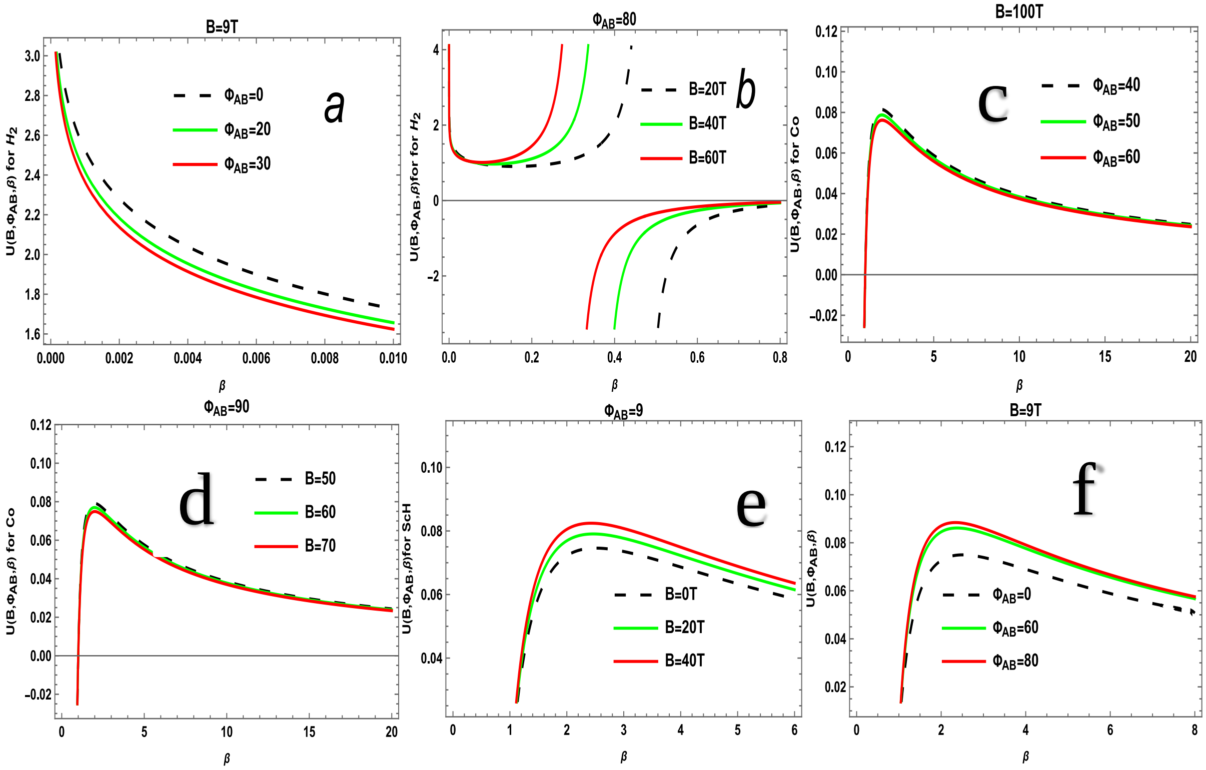

Figure 5: The plot of internal energy for three diatomic molecules varying magnetic field and Magnetic flux (Onate *et al.*, 2021).

As shown in Figure 5, Plot 5a illustrates that at a constant magnetic field of B=9 T, increasing the magnetic flux ϕ_{AB} results in lower internal energy values, particularly at low β (i.e., at high temperatures). The internal energy generally increases with β, indicating reduced thermal excitation at lower temperatures. In Plot 5b, with the magnetic flux fixed at ($\phi_{AB}=80$, the internal energy displays sharp variations and nonlinear behaviour. An increase in magnetic field strength leads to a sudden drop or divergence in internal energy at low β, highlighting the significant impact of strong magnetic fields on molecular energy levels (Onate *et al.*, 2021).

Plot 5c shows that at a fixed magnetic field of B=10 T, the internal energy increases with β, reaches a peak, and then gradually decreases. The influence of varying flux values is moderate but visible through the separation of the curves, suggesting that thermal saturation occurs at higher β. In Plot 5d, for $\phi_{AB}=90$, increasing the magnetic field causes the internal energy curves to peak and then decline slightly, implying that the magnetic field subtly adjusts the molecular energy distribution (Onate *et al.*, 2021).

In Plot 5e, with $\phi_{AB}=9$, internal energy rises sharply, reaches a maximum near β=2, and then declines. Here, higher magnetic fields correspond to reduced internal energy, emphasizing the suppressive effect of the field on energy levels. Finally, plot 5f, under a constant field of B=9 T and varying flux, exhibits a similar trend where internal energy peaks and then falls. As the magnetic flux increases, the internal energy decreases across the temperature range, reinforcing the role of flux in modulating thermal energy (Onate *et al.*, 2021).

The vibrational Free energy F(*β*) can be obtain as follows (Onate *et al.*, 2021)

$$F(\beta)=\frac{Log\left[\frac{e^{-k1\beta-\frac{k2k3\beta}{2}-\frac{1}{2}\sqrt{k2\beta}\sqrt{k2k3^2\beta}}\sqrt{\pi}\left(1-Erf\left[\frac{\sqrt{k2k3^2\beta}}{2\rho}-\frac{1}{2}\sqrt{k2\beta}\rho\right]+e^{\sqrt{k2\beta}\sqrt{k2k3^2\beta}}\left(-1+Erf\left[\frac{\sqrt{k2k3^2\beta}+\sqrt{k2\beta}\rho^2}{2\rho}\right]\right)\right)}{2\sqrt{k2\beta}}\right]}{\beta} \qquad (29)$$

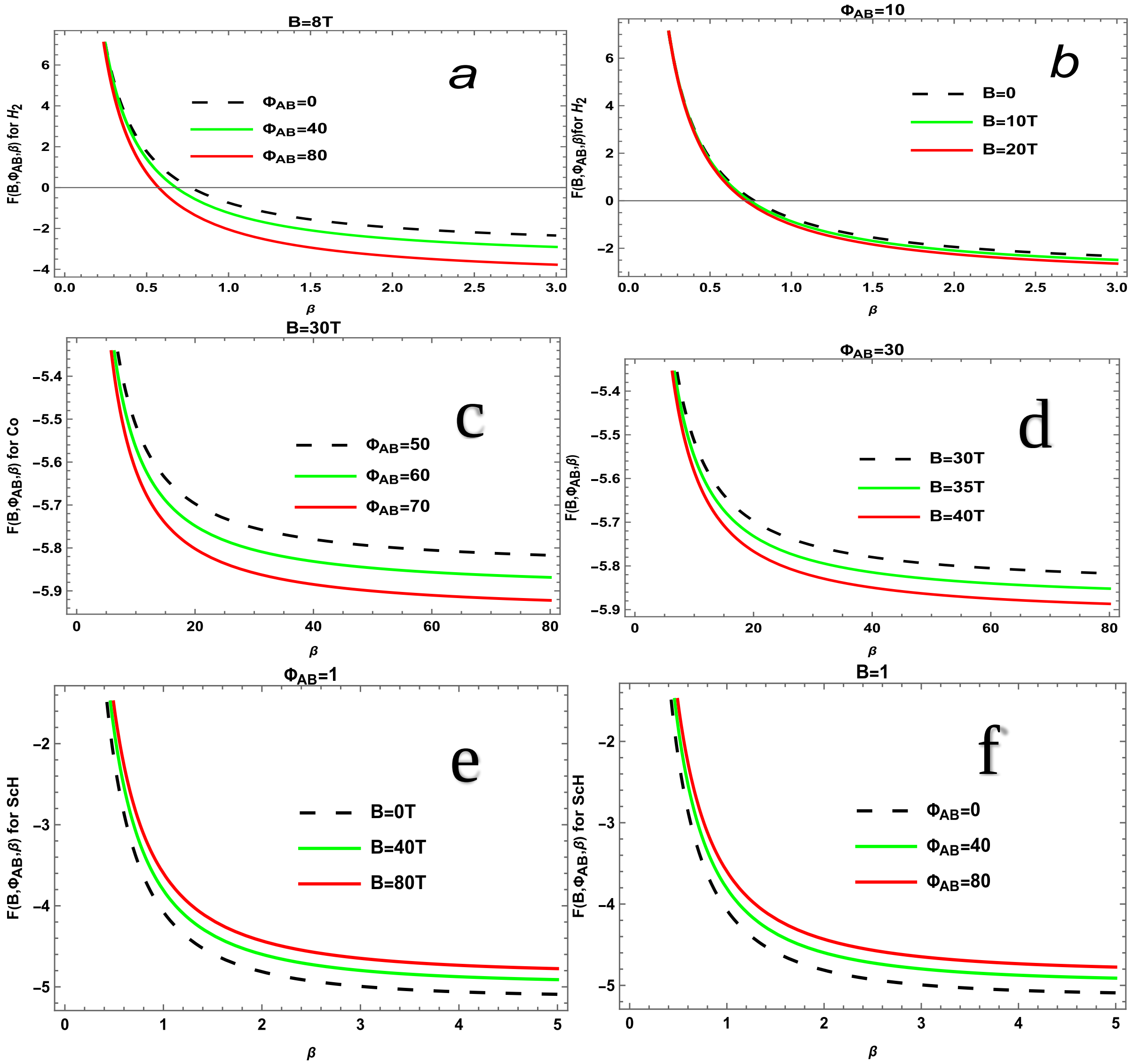

Figure 6: The plot of free energy for three diatomic molecules against temperature varying magnetic field and magnetic flux.

Figure 6 presents the variation of free energy with temperature under different magnetic field strengths and magnetic flux values. In plot 6a, at a constant magnetic field of B=8 T, it is evident that increasing the magnetic flux leads to a reduction in free energy, particularly at low values of temperature parameter β (corresponding to high temperatures). However, as temperature parameter β increases (lower temperatures), this difference becomes less significant. Plot 6b reveals that the free energy curves tend to converge at high temperature parameter β, suggesting that magnetic effects are more pronounced at lower temperature parameter β values (i.e., higher temperatures). In plot 6c, higher magnetic flux results in lower free energy, and the decreasing slope with increasing temperature parameter β reflects a flattening trend as the temperature drops. Plot 6d demonstrates that stronger magnetic fields lead to a reduction in free energy, with larger field strengths shifting the curve downward more noticeably at low temperature parameter β. In plot 6e, for a fixed magnetic flux $\phi_{AB} = 1$, increasing the magnetic field B consistently decreases the free energy. The curves become closer at higher temperature parameter β. Finally, plot 6f shows that the most significant variations in free energy occur at low temperature parameter β, highlighting the stronger thermal response in that region (Jia *et al.*, 2021).

The vibrational specific heat capacity $C(\beta)$ can be obtain as follows (Jia *et al.*, 2021)

$$C(\beta) = K\left(\frac{\partial^2 lnZ(\beta)}{\partial\beta^2}\right) \Rightarrow K_\beta \left[\frac{1}{8\beta^2}\left(-4 + D + E + \frac{F + G + H + 2P\sqrt{-\beta K_2}(I+J}{(P\sqrt{\pi}(1-e^{\sqrt{-\beta K_2}\sqrt{-\beta K_2 K_3^2}}+\gamma_1+\gamma_2))}\right)\right] \tag{30}$$

$$D = \frac{8e^{\sqrt{-\beta K_2}\sqrt{-\beta K_2 K_3^2}}(\gamma_3-\gamma_4)^2}{\pi(1-e^{\sqrt{-\beta K_2}\sqrt{-\beta K_2 K_3^2}}+\gamma_1+\gamma_2)^2 K_3^2} \tag{31}$$

$$\gamma_1 = e^{\sqrt{-\beta K_2}\sqrt{-\beta K_2 K_3^2}} Erf[\frac{P^2\sqrt{-\beta K_2}+\sqrt{-\beta K_2 K_3^2}}{2P}] \tag{32}$$

$$\gamma_2 = Erf[\frac{1}{2}P\sqrt{-\beta K_2} - \frac{\sqrt{-\beta K_2 K_3^2}}{2P}] \tag{33}$$

$$\gamma_3 = e^{\frac{1}{2}\sqrt{-\beta K_2}\sqrt{-\beta K_2 K_3^2}}\sqrt{\pi}\beta(-1 + \mathrm{Erf}[\frac{P^2\sqrt{-\beta K_2}+\sqrt{-\beta K_2 K_3^2}}{2P}])K_2 K_3^2 \tag{34}$$

$$\gamma_4 = e^{\frac{\beta K_2(P^4+K_3^2)}{4P^2}} P\sqrt{-\beta K_2 K_3^2} \tag{35}$$

$$E = \frac{\gamma_5-\gamma_6}{\sqrt{\pi}(1-e^{\sqrt{-\beta K_2}\sqrt{-\beta K_2 K_3^2}}+\gamma_1+\gamma_1)\sqrt{-\beta K_2}\sqrt{-\beta K_2 K_3^2}} \tag{36}$$

$$\gamma_5 = 2\beta(4e^{\sqrt{-\beta K_2}\sqrt{-\beta K_2 K_3^2}}\sqrt{\pi}\beta(-1 + \mathrm{Erf}[\frac{P^2\sqrt{-\beta K_2}+\sqrt{-\beta K_2 K_3^2}}{2P}])K_2^2 K_3^2 \tag{37}$$

$$\gamma_6 = 4e^{\frac{1}{4}(2\sqrt{-\beta K_2}\sqrt{-\beta K_2 K_3^2}+\frac{\beta K_2(P^4+K_3^2)}{P^2})} P K_2\sqrt{-\beta K_2 K_3^2} \tag{38}$$

$$F = 2e^{\frac{1}{2}\sqrt{-\beta K_2}\sqrt{-\beta K_2 K_3^2}}(-4e^{\frac{1}{2}\sqrt{-\beta K_2}\sqrt{-\beta K_2 K_3^2}} P\sqrt{\pi}\beta^2(-1 + \mathrm{Erf}[\frac{P^2\sqrt{-\beta K_2}+\sqrt{-\beta K_2 K_3^2}}{2P}])K_2^2 K_3^2 \tag{39}$$

$$G = e^{\frac{\beta K_2(P^4+K_3^2)}{4P^2}}\beta K_2(-P^4\sqrt{-\beta K_2} + \sqrt{-\beta K_2}K_3^2 + 4P^2\sqrt{-\beta K_2 K_3^2}) \tag{40}$$

$$I = e^{\frac{\beta K_2(P^4+K_3^2)}{4P^2}} P - 2e^{\frac{1}{2}\sqrt{-\beta K_2}\sqrt{-\beta K_2 K_3^2}}\sqrt{\pi}\sqrt{-\beta K_2 K_3^2} \tag{41}$$

$$J = 2e^{\frac{1}{2}\sqrt{-\beta K_2}\sqrt{-\beta K_2 K_3^2}}\sqrt{\pi}\mathrm{Erf}[\frac{P^2\sqrt{-\beta K_2}+\sqrt{-\beta K_2 K_3^2}}{2P}]\sqrt{-\beta K_2 K_3^2} \tag{42}$$

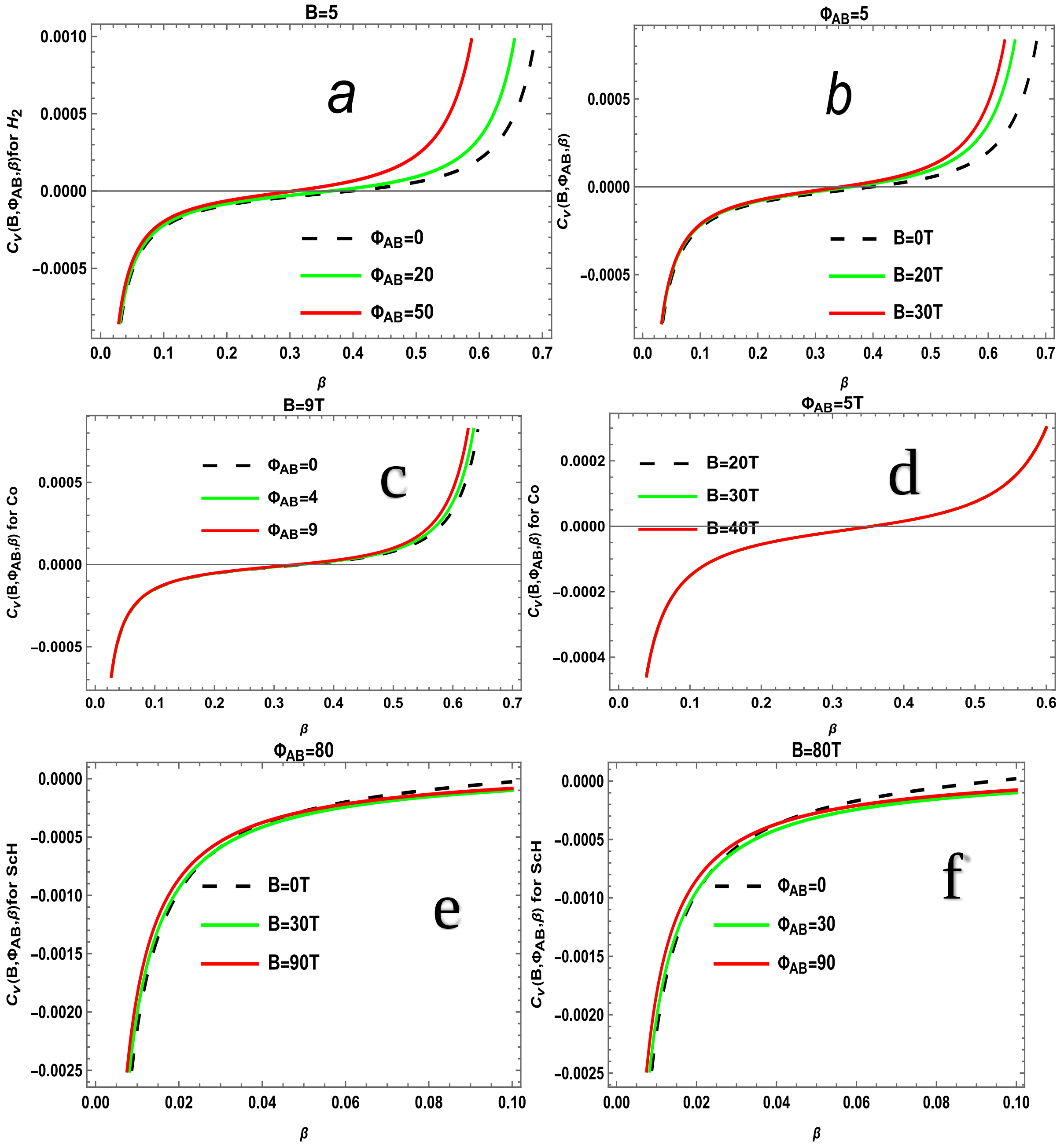

Figure 7: The plot of specific heat capacity for three diatomic molecules against absolute temperature varying magnetic field and magnetic flux.

Figure 7 displays the calculated values of specific heat capacity for three diatomic molecules under varying conditions. In plot 7a, the specific heat capacity $C_v$increases rapidly with the temperature parameter β, eventually reaching a steady state. Likewise, increasing the magnetic flux ϕ_{AB} also enhances C_v. In plot 7b, the effect of increasing the magnetic field B is observed to slightly reduce the computed values of C_v, indicating a subtle suppressive influence, whereas the impact of ϕ_{AB} appears less significant in this context.

Plot 7c illustrates that at a fixed magnetic flux $\phi_{AB} = 0$ the specific heat capacity increases at lower values of β (i.e., higher temperatures), with all magnetic field strengths B showing overlapping behaviour. This suggests that, in the absence of magnetic flux ϕ_{AB}, the specific heat capacity remains consistent across different magnetic fields.

In plot 7d, a slight divergence among the curves is noticeable at higher β (lower temperatures), implying convergence at elevated temperatures. This demonstrates that the influence of the magnetic field B on thermal behaviour is more apparent at low temperatures and becomes negligible as temperature increases.

From plot 7e, at a constant magnetic flux $\phi_{AB} = 10$, the curves corresponding to various magnetic field strengths begin to diverge gradually, with higher values of B producing marginally increased specific heat capacities.

Finally, plot 7f reveals that with the magnetic field set at B=0 T, both elevated magnetic flux and temperature contribute to a slight increase in the specific heat capacity C_v, (Umirzakoy, 1991).

The vibrational entropy $S(\beta)$ can be obtain as follows

$$S(\beta) = K_\beta\left(\frac{\left(-\frac{1}{\beta^2}\right)\left[Log\left[\frac{e^{\beta K_1+\frac{1}{2}\beta K_2K_3-\frac{1}{2}\sqrt{-\beta K_2}\sqrt{-\beta K_2K_3^2}}\sqrt{\pi}(P_1+P_2)}{2\sqrt{-\beta K_2}}\right]\right]+P_3+P_4+P_5+P_6}{(2P\sqrt{\pi}\beta^2P_1+(P_2)K_2^2\sqrt{-\beta K_2K_3^2})}\right)$$

(43)

$$P_1 = 1+e^{\sqrt{-\beta K_2}\sqrt{-\beta K_2K_3^2}}(-1+\mathrm{Erf}[\frac{P^2\sqrt{-\beta K_2}+\sqrt{-\beta K_2K_3^2}}{2P}])$$

(44)

$$P_2 = \mathrm{Erf}[\frac{1}{2}P\sqrt{-\beta K_2}-\frac{\sqrt{-\beta K_2K_3^2}}{2P}]$$

(45)

$$P_3 = ((P\sqrt{\pi}\beta(P_1)+P_2)K_2^2\sqrt{-\beta K_2K_3^2})$$

(46)

$$P_4 = K_2(-\beta K_2)^{3/2}(\gamma_7)K_2K_3^2 + 2e^{\frac{1}{4}(2\sqrt{-\beta K_2}\sqrt{-\beta K_2K_3^2}+\frac{\beta K_2(P^4+K_3^2)}{P^2})}P^2\sqrt{-\beta K_2K_3^2}) \qquad (47)$$

$$\gamma_7 = -2e^{\sqrt{-\beta K_2}\sqrt{-\beta K_2K_3^2}}P\sqrt{\pi}\beta(-1+\mathrm{Erf}[\frac{P^2\sqrt{-\beta K_2}+\sqrt{-\beta K_2K_3^2}}{2P}] \qquad (48)$$

$$P_5 = P\sqrt{\pi}P_1+P_2(-\beta K_2)^{3/2}(\beta K_2^2K_3^2 - 2K_1\sqrt{-\beta K_2}\sqrt{-\beta K_2K_3^2}+\frac{(-\beta K_2)^{3/2}K_3\sqrt{-\beta K_2K_3^2}}{\beta})$$

(49)

$$P_6 = (\frac{1}{\beta})'[\mathrm{Log}[\frac{e^{\beta K_1+\frac{1}{2}\beta K_2K_3-\frac{1}{2}\sqrt{-\beta K_2}\sqrt{-\beta K_2K_3^2}}\sqrt{\pi}(P_1+P_2)}{2\sqrt{-\beta K_2}}]]$$

(50)

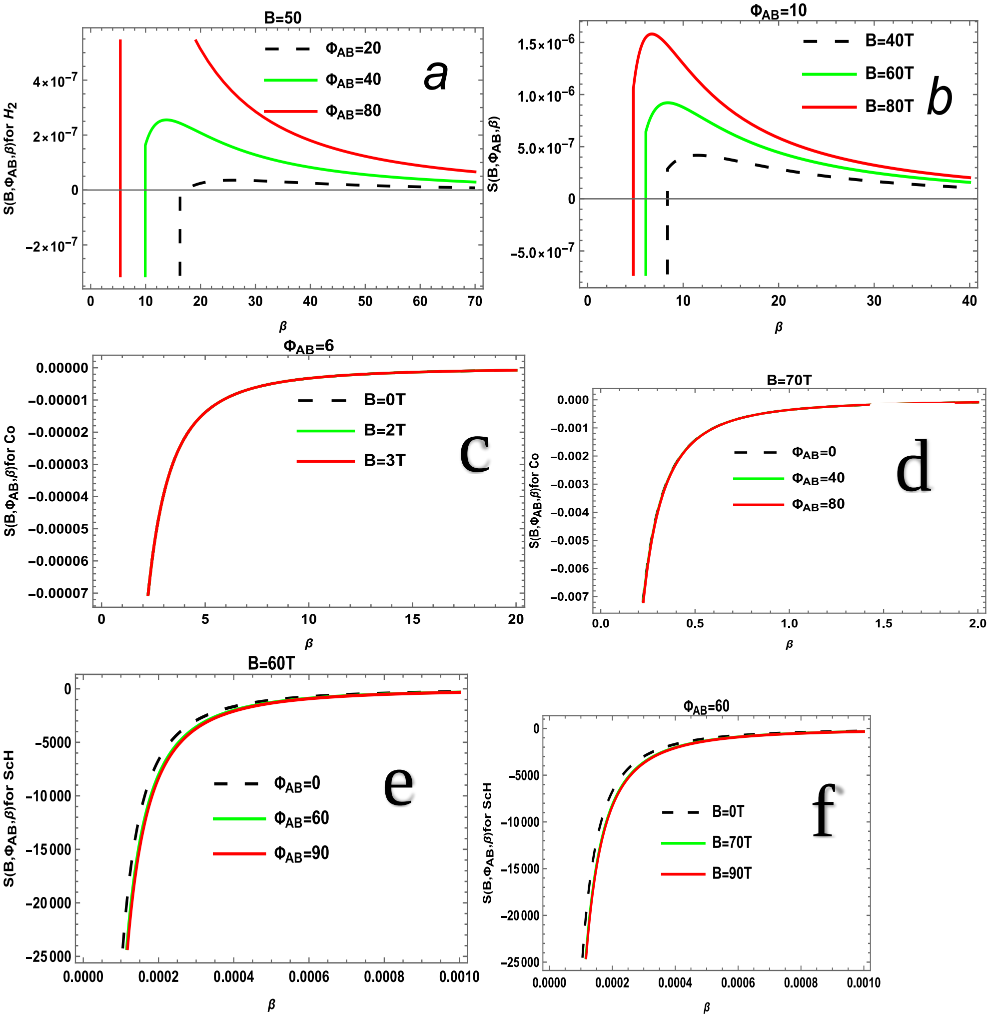

Figure 8: The plot of entropy for three diatomic molecules against temperature varying magnetic field and magnetic flux
.

Figure 8 presents six subplots (a–f), demonstrating the entropy behaviour of three diatomic molecules with respect to the inverse temperature (β), under varying magnetic field (B) and magnetic flux ϕ_{AB} conditions. Each subplot explores how entropy reacts to either changes in B or ϕ_{AB}. In plot 8a, increasing the magnetic flux ϕ_{AB} leads to noticeable shifts in entropy. Entropy rises rapidly with increasing β at lower values before stabilizing. Plot 8b indicates that when ϕ_{AB} is kept constant, increasing the magnetic field B causes entropy to increase, though the entropy curves tend to converge as β becomes larger. Plot 8c shows a sharp increase in entropy with rising β, eventually reaching a saturation point. This suggests that at very low values of both ϕ_{AB} and B, the system shows minimal sensitivity to magnetic field changes. In plot 8d, slight upward shifts in the entropy curves are observed with variations in ϕ_{AB}, signifying a modest but noticeable impact of magnetic flux, particularly at higher β. Plot 8e reveals that the curves behave almost identically, implying that the influence of ϕ_{AB} diminishes significantly at high β (low temperatures).

Finally, plot 8f demonstrates a steep initial rise in entropy followed by a plateau, with minimal differences between curves. This pattern indicates that magnetic field effects are more pronounced at low β (high temperatures) but become negligible as thermal ordering increases at higher β (Ettah, 2021).

The vibration energy fluctuation can calculate as follows (Ettah, 2021)

$$E_F[\beta] = K_\beta \beta^2 C_V[\beta]$$

(51)

$$E_F[\beta] = \beta^2 K_\beta K_\beta [\frac{1}{8\beta^2}\left(-4 + \frac{L+M+N+0+P+Q}{(P\sqrt{\pi}(1-e^{\sqrt{-\beta K_2}\sqrt{-\beta K_2 K_3^2}}+e^{\sqrt{-\beta K_2}\sqrt{-\beta K_2 K_3^2}}\gamma_8+Erf[\frac{1}{2}P\sqrt{-\beta K_2}-\frac{\sqrt{-\beta K_2 K_3^2}}{2P}]))}\right)$$

(52)

$$L = \frac{8e^{\sqrt{-\beta K_2}\sqrt{-\beta K_2 K_3^2}}(e^{\frac{1}{2}\sqrt{-\beta K_2}\sqrt{-\beta K_2 K_3^2}}\sqrt{\pi}\beta(-1+\gamma_8)K_2 K_3^2-e^{\frac{\beta K_2(P^4+K_3^2)}{4P^2}}P\sqrt{-\beta K_2 K_3^2})^2}{\pi(1-e^{\sqrt{-\beta K_2}\sqrt{-\beta K_2 K_3^2}}+e^{\sqrt{-\beta K_2}\sqrt{-\beta K_2 K_3^2}}\gamma_8+\mathrm{Erf}[\frac{1}{2}P\sqrt{-\beta K_2}-\frac{\sqrt{-\beta K_2 K_3^2}}{2P}])^2 K_3^2}$$

(53)

$$\gamma_8 = \mathrm{Erf}[\frac{P^2\sqrt{-\beta K_2}+\sqrt{-\beta K_2 K_3^2}}{2P}]$$

(54)

$$M = \frac{2\beta(4e^{\sqrt{-\beta K_2}\sqrt{-\beta K_2 K_3^2}}\sqrt{\pi}\beta(-1+\gamma_8)K_2^2 K_3^2-4e^{\frac{1}{4}(2\sqrt{-\beta K_2}\sqrt{-\beta K_2 K_3^2}+\frac{\beta K_2(P^4+K_3^2)}{P^2})}PK_2\sqrt{-\beta K_2 K_3^2})}{\sqrt{\pi}(1-e^{\sqrt{-\beta K_2}\sqrt{-\beta K_2 K_3^2}}+e^{\sqrt{-\beta K_2}\sqrt{-\beta K_2 K_3^2}}\gamma_8+\mathrm{Erf}[\frac{1}{2}P\sqrt{-\beta K_2}-\frac{\sqrt{-\beta K_2 K_3^2}}{2P}])\sqrt{-\beta K_2}\sqrt{-\beta K_2 K_3^2}}$$

(55)

$$N = 2e^{\frac{1}{2}\sqrt{-\beta K_2}\sqrt{-\beta K_2 K_3^2}}(-4e^{\frac{1}{2}\sqrt{-\beta K_2}\sqrt{-\beta K_2 K_3^2}}P\sqrt{\pi}\beta^2(-1 + \mathrm{Erf}[\frac{P^2\sqrt{-\beta K_2}+\sqrt{-\beta K_2 K_3^2}}{2P}])K_2^2 K_3^2)$$

(56)

$$O = e^{\frac{\beta K_2(P^4+K_3^2)}{4P^2}}\beta K_2(-P^4\sqrt{-\beta K_2} + \sqrt{-\beta K_2}K_3^2 + 4P^2\sqrt{-\beta K_2 K_3^2})$$

(57)

$$P = 2P\sqrt{-\beta K_2}\, e^{\frac{\beta K_2\left(P^4+K_3^2\right)}{4P^2}}P - 2e^{\frac{1}{2}\sqrt{-\beta K_2}\sqrt{-\beta K_2 K_3^2}}\sqrt{\pi}\sqrt{-\beta K_2 K_3^2}$$

(58)

$$Q = 2e^{\frac{1}{2}\sqrt{-\beta K_2}\sqrt{-\beta K_2 K_3^2}}\sqrt{\pi}\mathrm{Erf}[\frac{P^2\sqrt{-\beta K_2}+\sqrt{-\beta K_2 K_3^2}}{2P}]\sqrt{-\beta K_2 K_3^2}$$

(59)

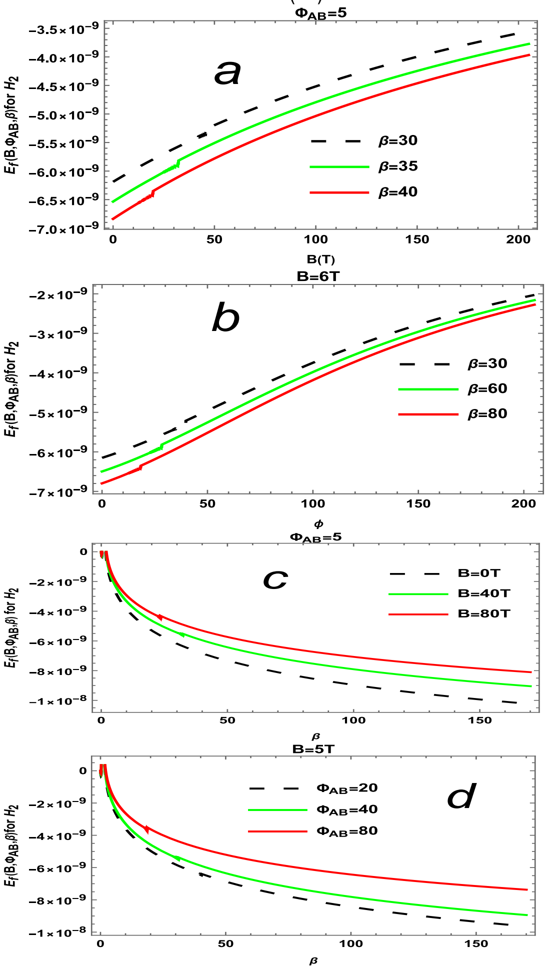

Figure 9: The plot for energy fluctuation of Hydrogen diatomic molecule varying temperature, magnetic field and magnetic flux**.**

Figure 9 reveals a distinct trend in energy fluctuation behaviour as influenced by variations in magnetic field B and magnetic flux ϕ_{AB} across a temperature range (β = 0 to 80). In plot 9a, an increase in the magnetic field B leads to a rise in energy fluctuations at different values of the temperature parameter β. Plot 9b indicates that changes in magnetic flux ϕ_{AB} affect the energy fluctuation levels as β varies. In plot 9c, it is observed that as β increases, energy fluctuations decrease under different magnetic field strengths B. A similar trend is evident in plot 9d, where rising values of β correspond to a decline in energy fluctuations when the magnetic flux ϕ_{AB} varies (Ikot et al., 2021).

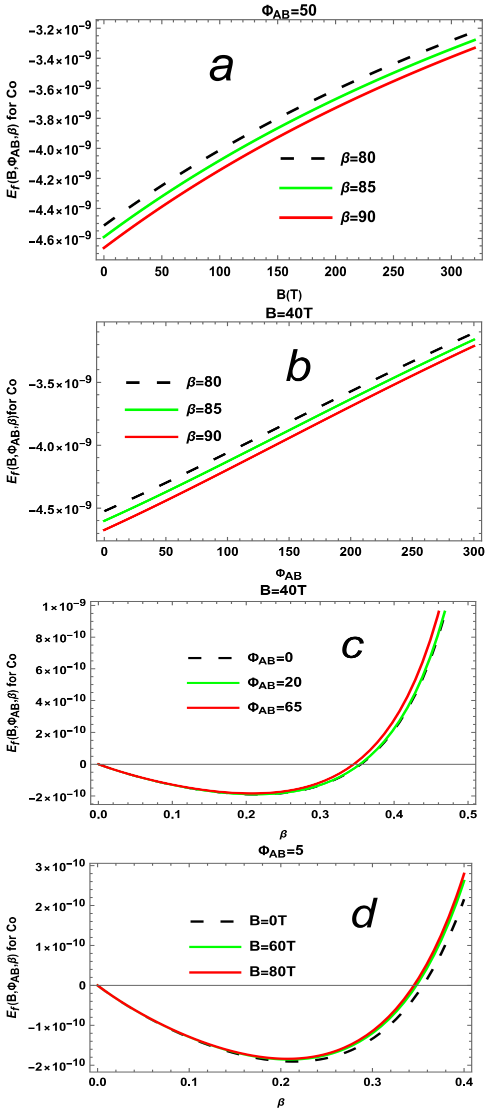

Figure 10: The plot for energy fluctuation of Carbon - monoxide diatomic molecule varying temperature, magnetic field and magnetic flux.

Figure 10 illustrates the behavior of energy fluctuation under various conditions. In plot 10a, with the magnetic flux $\phi_{AB} = 50$, the energy fluctuation of carbon monoxide increases as the magnetic field strength rises. Plot 10b reveals that as the magnetic flux ϕ_{AB} increases, the energy fluctuation also increases under different values of the temperature parameter β. Similarly, plot 10c demonstrates that greater values of β lead to a corresponding rise in energy fluctuation when the magnetic flux varies. Lastly, plot 10d shows that for carbon monoxide, the computed energy fluctuation increases with the temperature parameter β.

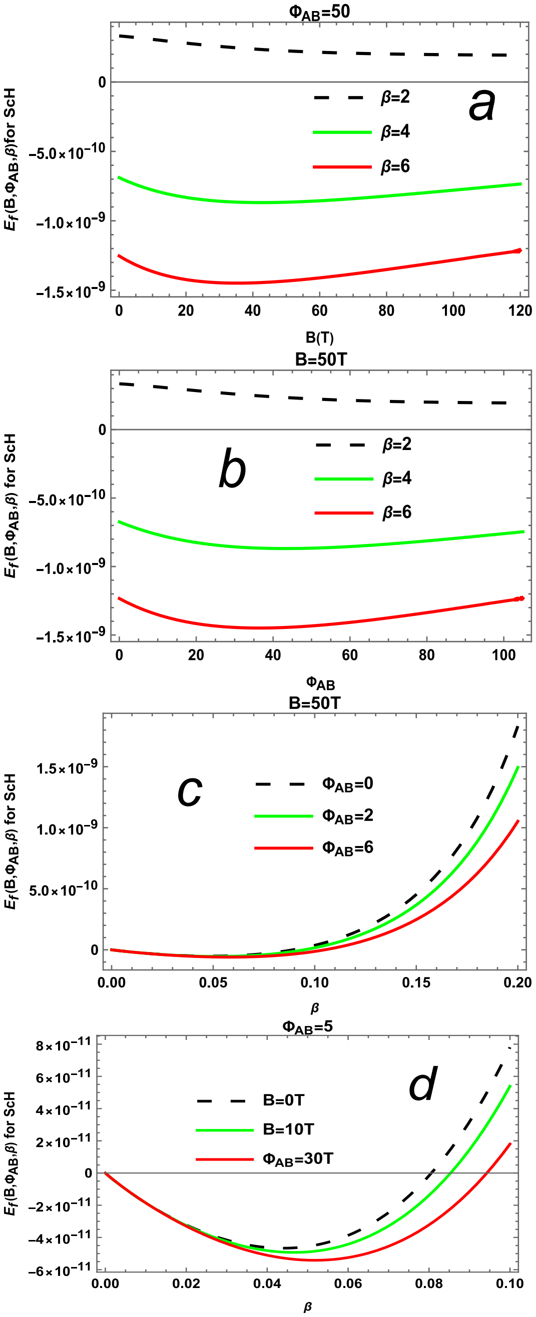

Figure 11: The plot for energy fluctuation of scandium hydride molecules varying temperature, magnetic field and magnetic flux.

Figure 11 presents the energy fluctuation behavior of Scandium Hydride as a function of the inverse temperature, expressed as $\beta = \frac{1}{K_{\beta}T}$ (j^{-1}),, under varying conditions of magnetic field B and magnetic flux ϕ_{AB}. In Plot 11a, a slight curvature is observed initially; however, as both the magnetic field and temperature parameter increase, the curve becomes steeper, indicating a rise in the calculated energy fluctuation. Plot 11b reveals a nearly linear increase in energy fluctuation with rising magnetic flux ϕ_{AB} across a range of β values. In Plot 11c, an upward trend in energy fluctuation is seen as the temperature parameter increases under different levels of magnetic flux. Finally, plot 11d demonstrates that increasing the magnetic field leads to greater energy fluctuation, particularly at higher values of the temperature parameter.

Conclusion

This analysis highlights the profound impact of external magnetic fields and flux on molecular energy dynamics. The NUFA method provides a robust framework for solving the Schrödinger equation in such complex scenarios, offering insights into the interplay between quantum mechanics and external influences.

REFERENCES

Abu-Shady, M., & Khokha, E. M. (2023). A precise estimation for vibrational energies of diatomic molecules using the improved Rosen–Morse potential. *Scientific Reports*, *13*(1), 11578.

Ding, Y., & Wang, Z. Q. (2011). Bound states of nonlinear Schrödinger equations with magnetic fields. *Annali di Matematica Pura ed Applicata*, *190*(3), 427-451.

Dong, S. H. (2000). Exact solutions of the two-dimensional Schrödinger equation with certain central potentials. *International Journal of Theoretical Physics*, *39*, 1119-1128.

Edet, C. O., Amadi, P. O., Onyeaju, M. C., Okorie, U. S., Sever, R., Rampho, G. J., ... & Ikot, A. N. (2021). Thermal properties and magnetic susceptibility of Hellmann potential in Aharonov–Bohm (AB) flux and magnetic fields at zero and finite temperatures. *Journal of Low Temperature Physics*, *202*, 83-105.

Ettah, E. (2021). The Schrödinger Equation with Deng-Fan-Eckart Potential (DFEP): Nikiforov-Uvarov-Functional Analysis (NUFA) Method. *European Journal of Applied Physics*, *3*(5), 58-62.

Ikot, A. N., Okorie, U. S., Amadi, P. O., Edet, C. O., Rampho, G. J., & Sever, R. (2021). The Nikiforov–Uvarov-Functional Analysis (NUFA) Method: A new approach for solving exponential-type potentials. *Few-Body Systems*, *62*, 1-16.

Jia, C. S., Diao, Y. F., Liu, X. J., Wang, P. Q., Liu, J. Y., & Zhang, G. D. (2012). Equivalence of the Wei potential model and Tietz potential model for diatomic molecules. *The Journal of chemical physics*, *137*(1).

Manga, P. J., Buteh, S. D., Maina, M., Amusat, R. O., Teru, P. B., Hashimu, M. U., & John, D. S. (2023). Solutions of Schrödinger equation based on Modified Exponential Screened Plus Yukawa Potential (MESPYP) within the frame of parametric Nikiforov-Uvarov method. *Dutse Journal of Pure and Applied Sciences*, *9*(3b), 144-154.

Manga, P. J., Likta, E. W., & Teru, P. B. (2021). Comparative Study on Charged and Neutral Pion-Nucleon Coupling Constants Using Yukawa Potential Model. *FUDMA JOURNAL OF SCIENCES*, *5*(4), 167-173.

Onate, C., Okon, I. B., Onyeaju, M. C., & Antia, A. D. (2022). Approximate solutions of the Schrodinger Equation for a Momentum-Dependent potential. *Journal of the Nigerian Society of Physical Sciences*, 242-250.

Reiss, H. R. (1980). Effect of an intense electromagnetic field on a weakly bound system. *Physical Review A*, *22*(5), 1786.

Umirzakov, I. (2019). Incorrectness of analytical solution of Schrodinger equation for diatomic molecule with shifted Tietz-Wei potential. *arXiv preprint arXiv:1902.04977*.